ACS NANO
Cite This: ACS Nano 2019, 13, 13264−13270
www.acsnano.org

ARTICLE

Ultrafast Exciton Trapping at sp^3 Quantum Defects in Carbon Nanotubes

Matthew E. Sykes,[†] Mijin Kim,[‡] Xiaojian Wu,[‡] Gary P. Wiederrecht,[†] Lintao Peng,[†] YuHuang Wang,[‡] David J. Gosztola,[†] and Xuedan Ma*[,†]

[†]Center for Nanoscale Materials, Argonne National Laboratory, Lemont, Illinois 60439, United States
[‡]Department of Chemistry and Biochemistry, University of Maryland, College Park, Maryland 20742, United States

Supporting Information

ABSTRACT: Semiconducting single-walled carbon nanotubes (SWCNTs) constitute an ideal platform for developing near-infrared biosensors, single photon sources, and nanolasers due to their distinct optical and electrical properties. Covalent doping of SWCNTs has recently been discovered as an efficient approach in enhancing their emission intensities. We perform pump−probe studies of SWCNTs that are covalently doped with sp^3 quantum defects and reveal strikingly different exciton formation dynamics and decay mechanisms in the presence of the defect sites. We show that, in highly doped SWCNTs, ultrafast trapping of excitons at the defect sites can outpace other photodynamic processes and lead to ground-state photobleaching of the quantum defects. Our fitting of the transient data with a kinetic model also reveals an upper limit in the quantum defect density for obtaining highly luminescent SWCNTs without causing irreversible damage. These findings not only deepen our understanding of the photodynamics in covalently doped SWCNTs but also reveal critical information for the design of bright near-infrared emitters that can be utilized in biological, quantum information, and nanophotonic applications.

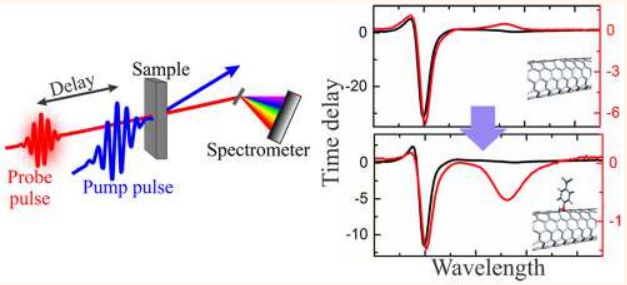

KEYWORDS: *single-walled carbon nanotubes, quantum defects, pump−probe spectroscopy, ground-state photobleaching, stimulated emission, exciton trapping*

Covalent doping of single-walled carbon nanotubes (SWCNTs) with aryl or alkyl functional groups[1−3] introduces sp^3 quantum defects that manifest themselves as deep trapping states capable of capturing excitons even at room temperature.[4,5] Such a localization of excitons significantly reduces the possibility of excitons recombining nonradiatively at quenching sites and leads to red-shifted emission and a drastically enhanced photoluminescence (PL) quantum efficiency.[1,6] Localization of excitons in the quantum defects also enables room-temperature single photon emission at telecom wavelengths.[2,7] Moreover, the deep trapping states associated with the quantum defects in a one-dimensional system may serve as an efficient three-level structure for accumulating excitons and realizing a population inversion (Figure 1d). When pumped nonresonantly, the quantum defect states in the doped SWCNTs are populated by the diffusive transport of excitons generated in the undoped segments of SWCNTs.[8,9] As a result, emission from the quantum defects is related to not only the oscillator strength of the associated optical transitions but also the photodynamic processes in the SWCNTs. Specifically, exciton−exciton annihilation and diffusive quenching diminish the populations of excitons in the SWCNTs and compete with the capture of excitons in the quantum defects. In situations where localization of excitons in the quantum defects outpaces the other processes, saturation of the quantum defect states may occur, potentially leading to stimulated emission from the sp^3 quantum defects. Understanding the diffusion, recombination, and trapping dynamics of excitons in covalently doped SWCNTs is therefore essential for their many photonic and optoelectronic applications.[10−12]

In this paper, we perform pump−probe studies of SWCNTs that are covalently doped with sp^3 quantum defects and reveal strikingly different exciton formation dynamics and decay mechanisms in the presence of the defect sites. We show that, in covalently doped SWCNTs, ultrafast photodynamic processes are greatly dependent on the quantum defect concentrations. At high quantum defect densities, the ultrafast trapping of excitons at the quantum defect sites can outpace other photodynamic processes and become the dominant

Received: August 8, 2019
Accepted: October 29, 2019
Published: October 29, 2019

DOI: 10.1021/acsnano.9b06279
ACS Nano 2019, 13, 13264−13270

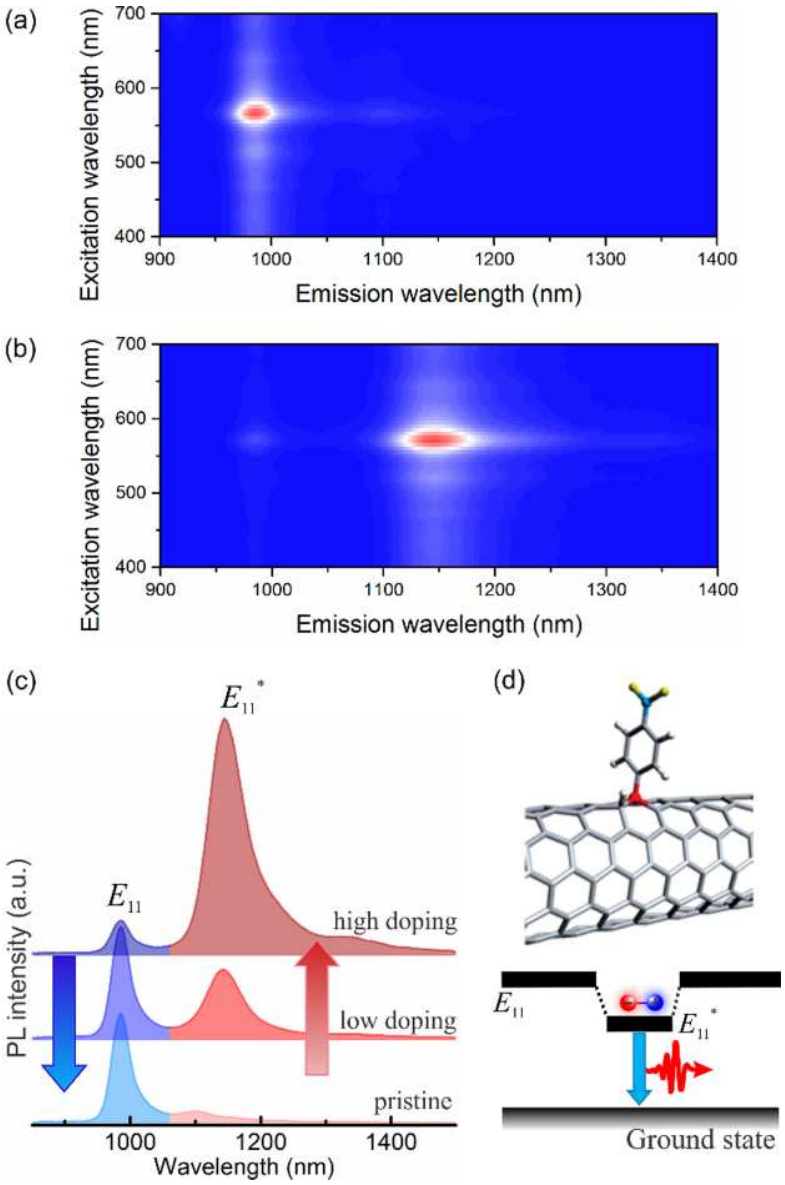

Figure 1. (a,b) Excitation wavelength-dependent photoluminescence spectra of pristine (a) and highly doped (b) (6,5) SWCNTs. Doping of (6,5) SWCNTs with 4-nitrobenzenediazonium tetrafluoroborate gives rise to a bright, red-shifted peak at around 1160 nm. (c) Doping concentration-dependent photoluminescence spectra of SWCNTs for an excitation wavelength of 565 nm. Concentrations of SWCNTs in the three samples are kept the same. (d) Molecular structure and the related energy levels of an sp^3 quantum defect in a covalently doped (6,5) SWCNT.

decay channel, leading to ground-state photobleaching of the quantum defects. These findings provide valuable information for enhancing SWCNT brightness and generating stimulated emission from the defects.

RESULTS AND DISCUSSION

Chirality-sorted (6,5) SWCNTs with band-edge excitons (the so-called E_{11} excitons) emitting at around 985 nm and with an average length of 350 nm (Supporting Information S1) are covalently doped by an aryl diazonium salt, 4-nitrobenzenediazonium tetrafluoroborate (see Methods for the details).[1] This gives rise to a red-shifted PL peak centered at about 1160 nm, corresponding to the sp^3 quantum defect state (noted as the E_{11}^* state) (Figure 1a,b). The PL intensity ratio of E_{11}^* excitons relative to E_{11} excitons increases with the doping concentration in a certain range (Figure 1c), but a further increase in the doping concentration leads to an irreversible PL quenching (Supporting Information S1). An increase in the disorder with the defect density is also reflected in the D-band in the Raman spectra (Supporting Information S1).

To understand the carrier dynamics of the covalently doped SWCNTs, femtosecond transient absorption (TA) spectra of the SWCNTs were measured by resonant pumping of the E_{11} state at 980 nm and probing with a continuum pulse spanning the near-infrared (Figure 2a). A Ti:sapphire laser with a regeneratively amplified 800 nm output pulse at 5 kHz was used, 95% of which was coupled to an OPA to produce a pump beam with a wavelength of 980 nm. The remaining 5% of the amplified pulse was sent through a delay line and focused onto a sapphire crystal to generate a continuum probe pulse

DOI: 10.1021/acsnano.9b06279
ACS Nano 2019, 13, 13264−13270

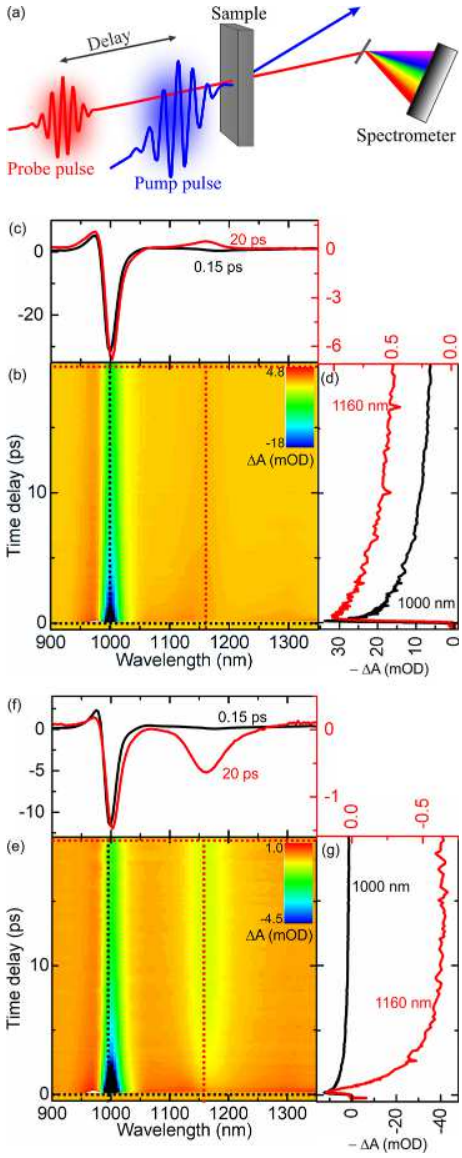

Figure 2. (a) Schematic representation of the pump−probe setup. An ultrafast near-infrared pump pulse (980 nm) is focused onto a SWCNT sample, which is probed with a continuum pulse spanning the near-infrared. The spectra of the probe pulse through the sample are measured by a spectrometer. (b,e) Two-dimensional plots of TA spectra from pristine (b) and highly doped (e) SWCNTs showing the pump-induced differential absorption (ΔA) as functions of probe photon wavelength and pump−probe time delay. Pump powers of (b,e) are 25 and 15 μW, respectively. (c,f) TA spectra at specific delay times obtained by horizontal cuts through the two-dimensional TA data in (b,e). (d,g) Kinetics at specific probe photon wavelengths obtained by vertical cuts through the two-dimensional TA data. Note that for easy comparison, the sign in (d,g) are inverted to $-\Delta A$.

extending from 850 to 1600 nm. The pump beam was depolarized to avoid rotational anisotropy impacts on the TA signal. Both beams were focused at near-normal incidence to a ~200 μm spot and spatially overlapped on the samples. The transmitted beam was fiber-coupled to a spectrometer with an InGaAs array detector. The pulse width of the pump beam was determined to be 120.7 ± 7.3 fs by pumping toluene at 980 nm and measuring a Raman line near 1400 nm.

Two-dimensional plots of TA spectra from pristine SWCNTs showing the pump-induced differential absorption (ΔA) as a function of probe photon wavelength and pump−probe time delay are presented in Figure 2b. Horizontal cuts through the two-dimensional TA data in Figure 2b yield spectra at specific delay times (Figure 2c). The predominant feature is a photon excitation induced ground-state bleaching signal centered at the E_{11} peak. The blue-shifted positive ΔA signal with respect to the photobleaching signal has been attributed to photon-induced absorption caused by the excitation of dark singlet excitons[13] or formation of biexcitons.[14] Note that the photoinduced absorption band at around 1160 nm is caused by the formation of trions through an Auger process,[15,16] in which recombination energy from one exciton is transferred to another, causing its dissociation and leading to the formation of charge carriers in the SWCNTs. Subsequent photon excitation of the charge carriers by the probe pulse leads to the formation of trions and an induced absorption.[15,17] The other photoinduced absorption features centered at 1100 and 1300 nm have been observed before and are assigned to different origins.[18,19]

The TA spectrum of a highly doped SWCNT sample with a nominal doping concentration of $N_{D,theo}$ = 16 quantum defects per tube (see Supporting Information S2 for the calculation of doping concentrations) (Figure 2e) shows features similar to those of the pristine tubes upon initial excitation but exhibits an additional negative ΔA signal and increase in the probe transmission at around 1160 nm at longer time delays (Figure 2g). The transient spectra of this signal (Figure 2f) overlap well with the defect absorption and emission in the steady-state absorption and PL spectra (Figures 1b,c, and S1). Based on these observations, this negative ΔA signal could have two potential origins:[20] ground-state photobleaching of the quantum defects, inferring a reduction of the available ground-state populations due to excitation from the pump, and/or stimulated emission from the E_{11}^* state in the quantum defects. During the stimulated emission process, an incoming probe photon induces emission of another photon from the E_{11}^* state, with the stimulated photon emitting in the same direction as the probe photon, hence producing an increased detected signal. This kind of stimulated emission has been observed in materials with large optical gains including organic dye molecules,[21] conjugated polymers,[22] and semiconductor quantum dots[23] and is a prerequisite for obtaining optical gain and lasing. A closer comparison of the SWCNT absorbance at the E_{11}^* peak (Figure S1b) and the maximum transmission corresponding to the negative ΔA signal (Figure S6) shows a slightly larger absorbance (~5 mOD) compared to that of the probed transmission (~1.5 mOD), indicating that ground-state photobleaching instead of stimulated emission is the main contribution to the observed negative ΔA signal, and no optical gain is achieved. We note, though, that this negative ΔA signal overlaps with the photon-induced absorption peak due to trion formation (Figure 2c). The latter compensates contributions from any potential stimulated emission. We therefore expect that in order to obtain dominant stimulated emission and enable optical gain from the quantum defects, it is beneficial to tune the E_{11}^* state away from the trion absorption peak, which is achievable by adapting SWCNTs with a different diameter or doping group.[1,2] The transient feature at 1160 nm (Figure 3b) reveals that the ground-state photobleaching process associated with the formation of the

DOI: 10.1021/acsnano.9b06279
ACS Nano 2019, 13, 13264−13270

E_{11}^* excitons occurs very rapidly (within 600 fs when ΔA turns negative).

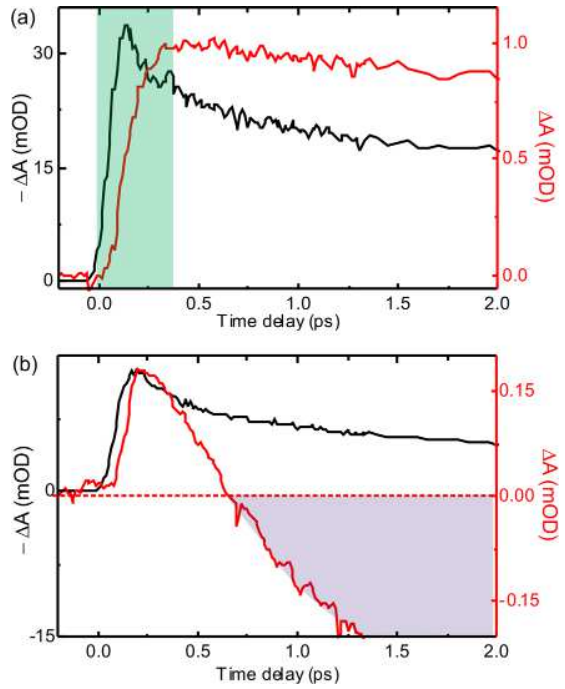

Figure 3. Kinetics of pristine (a) and highly doped (b) SWCNTs at 1000 nm (black curves) and 1160 nm (red curves) in the first 2 ps. Pump powers of (a,b) are 25 and 15 μW, respectively. The highlighted area in (a) denotes the correlation between the E_{11} exciton decay and the rise of the nascent trion signal within the first 0.5 ps, which indicates the Auger process related formation mechanism of the trions. The highlighted area in (b) shows the regime where the ΔA signal from the doped SWCNTs at 1160 nm (red) turns negative, indicating a photobleaching of the quantum defect ground state.

As mentioned above, when pumped nonresonantly, E_{11}^* states are populated by diffusive transport of excitons generated in the undoped segments of SWCNTs.[8,9] Therefore, the formation dynamics of E_{11}^* excitons are determined by the competition between trapping of excitons in the quantum defects and other decay channels (mainly including first-order exciton decay, exciton−exciton annihilation, and trion formation[15,16]), as depicted in Figure 4a. To reveal the competing mechanisms among these channels, we fit the pump-power-dependent two-dimensional TA data with numerical solutions of coupled differential equations that describe the kinetic model (see Supporting Information S3 for the detailed fitting method). To investigate the influence of doping concentration, four different samples were studied, including a pristine SWCNT sample and three doped SWCNT samples with nominal doping concentrations $N_{D,theo}$ of 3, 16, and 314 quantum defects per tube. In this model, we consider diffusion-limited E_{11} exciton decay and exciton−exciton annihilation processes. To account for the optically generated trions at 1160 nm, we adapt an Auger recombination mechanism.[15,16] In this process, photoexcitation of charge carriers generated by Auger recombination leads to the formation of trions. This assumption is in agreement with the correlation between the E_{11} exciton decay and the rise of the nascent trion signal within the first 0.5 ps in Figure 3a.

Fitting of transients at different pump intensities and wavelengths are shown in Figure 4b−e and Supporting Information S4, and an excellent agreement between the model and the experimental data can be observed. This model enables us to derive a single set of photodynamic parameters that describe all of the measured TA spectra regardless of doping concentrations. For the E_{11} excitons in pristine tubes, we obtain a time-dependent exciton−exciton annihilation constant of $k_a = \frac{1}{2}k_{EEA}t^{-1/2} = 2.8 \times 10^6 t^{-1/2}$ nm s$^{-1/2}$, which corresponds to an exciton diffusion constant[24] D of 0.05 cm^2/s, close to the values obtained previously by TA[25] and fluorescence quenching measurements.[15] From the E_{11} exciton decay time τ_1 = 4.3 ps, we derive an exciton diffusion length of L = 4.7 nm in the pristine tubes, in agreement with previously reported values of similar SWCNT systems studied by transient absorption spectroscopy.[25] Upon doping, the diffusion length of the E_{11} excitons decreases slightly to 4.2 nm for the sample doped with $N_{D,theo}$ = 3 defects/tube and 4.0 nm for the one with $N_{D,theo}$ = 16 defects/tube. This diffusion length is still much shorter than the average distance between two quantum defects of 29 nm in the highly doped SWCNTs (see Supporting Information S5 for the detailed calculations), indicating that the doping concentration can be further increased before destructive effects to the SWCNTs happen. If we assume the exciton diffusion length as the limiting factor and any SWCNT with a quantum defect separation less than the exciton diffusion length would have a quenched PL, we obtain an approximate upper limit in the quantum defect density of around 88 defects/tube. This finding is consistent with our observation of irreversible quenching at a doping concentration of 314 defects/tube. In this case, the distance between two quantum defects (1.1 nm) is actually smaller than the size of excitons in SWCNTs (~2.0 nm[25]). On the other hand, the low doping concentration ($N_{D,theo}$ = 3 defects/tube) has a minimal influence on the photodynamics of the SWCNTs due to the predominant contributions from the E_{11} excitons, as can be seen from the two-dimensional plot of TA spectra in Supporting Information S4 and pump-dependent photobleach signals shown in Supporting Information S6. In this case, the doping density is low enough that other competing channels such as trion formation dominate the E_{11} exciton decay process before trapping by the quantum defects may occur.

The diffusion-limited exciton trapping model yields an exciton trapping rate $k_D = k_{Tr}t^{-1/2}N_D$ of 2×10^6 $t^{-1/2}$ nm s$^{-1/2}$ for the weakly doped SWCTNs with $N_{D,theo}$ = 3 defects/tube and $5 \times 10^7 t^{-1/2}$ nm s$^{-1/2}$ for the highly doped SWCNTs with $N_{D,theo}$ = 16 defects/tube. This fast trapping rate in the highly doped SWCNTs indicates that, at pump intensities below the saturation of the E_{11} photobleaching signals (see Supporting Information S7), E_{11} excitons, right after their generation, are most likely to be captured at a nearby quantum defect within their diffusion range rather than undergoing annihilation or Auger processes. In other words, when the density of the E_{11} excitons $N_{E_{11}}$ is kept below 18 excitons/tube, the exciton trapping rate $k_D = k_{Tr}t^{-1/2}N_D$ is always larger than the exciton−exciton annihilation rate $k_A = \frac{1}{2}k_{EEA}N_{E_{11}}t^{-1/2}$. This fast trapping rate, together with the long lifetime of the E_{11}^* states (~100 ps[4,7,9]), leads to an accumulation of excitons in the quantum defect states and depletion of the ground state, explaining the observation of the negative ΔA signal observed

DOI: 10.1021/acsnano.9b06279
ACS Nano 2019, 13, 13264−13270

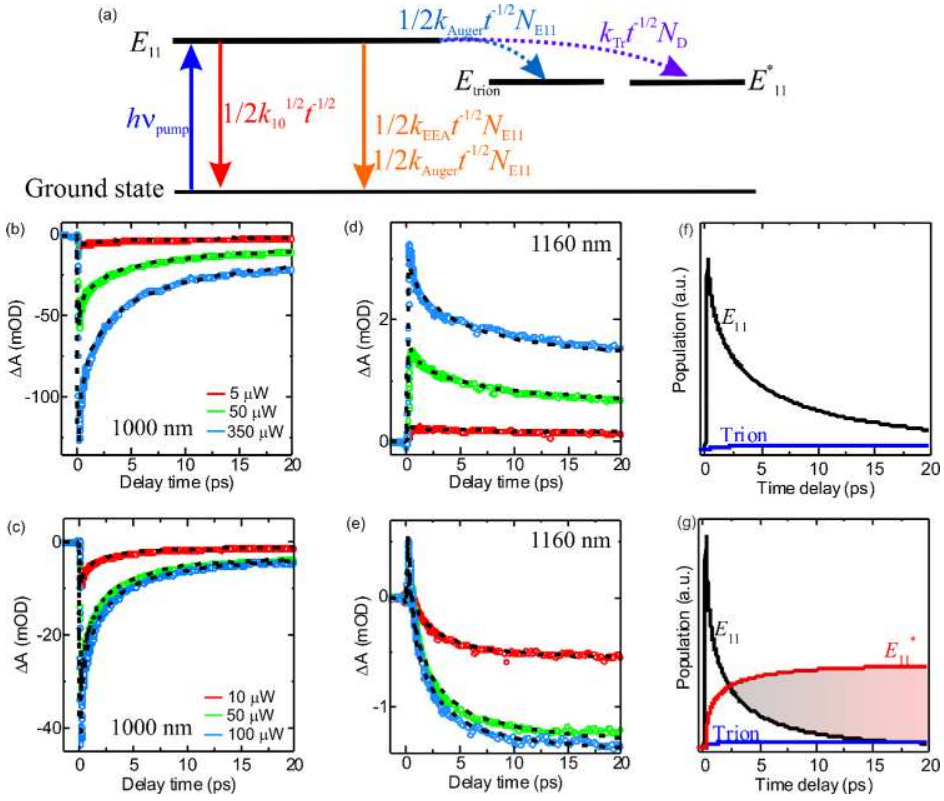

Figure 4. (a) Diagrammatic representation of the kinetic model that is used to describe the main decay channels in the SWCNTs. The decay rate of each channel is indicated. E_{11} excitons in the doped SWCNTs mainly decay through four channels: first-order decay (k_{10}), exciton−exciton annihilation (k_{EEA}), trion formation *via* Auger process (k_{Auger}), and trapping at quantum defects (k_{Tr}). (b−e) Circles: Pump-intensity-dependent kinetic traces of the pristine (b,d) and highly doped (c,e) SWCNTs at the E_{11} (b,c) and E^*_{11} (d,e) bands. Dashed curves: Corresponding fittings applying the kinetic model discussed in the text. (f,g) Numerically simulated population evolutions of E_{11} excitons (black), trions (blue), and E^*_{11} excitons (red) in pristine SWCNTs (f) and highly doped SWCNTs (g). The pump powers are set at 25 μW for both the pristine and highly doped SWCNTs. In the pristine SWCNTs, the population of E_{11} excitons dominates. In the highly doped SWCNTs, the E^*_{11} exciton population dominates over that of the E_{11} excitons within 3 ps, indicating the bleaching of the ground state (the highlighted area in (g)).

in the TA spectra of highly doped SWCNTs. This conclusion is further supported by the saturation of the maximum E^*_{11} state ΔA signals at high pump intensities (Supporting Information S6).

To obtain a more intuitive understanding of the carrier dynamics in the measured time window, we extract the population densities from the TA fittings and find that E_{11} excitons dominate the excited-state populations in the pristine SWCNTs (Figure 4f). In contrast, in the highly doped SWCNTs, the population of E^*_{11} excitons outnumbers that of the E_{11} excitons within 3 ps after optical excitation (Figure 4g). Of the four E_{11} exciton decay channels (first-order decay, exciton−exciton annihilation, trion formation *via* Auger process, and trapping at quantum defects), exciton trapping at quantum defects represents the main decay channel for the highly doped SWCNTs. Meeting this condition is critical for generating optical gain from quantum defects in SWCNTs, provided that their stimulated emission can outcompete reabsorption by states such as trion.

CONCLUSIONS

In summary, we find that exciton dynamics in covalently doped SWCNTs are strongly affected by the presence and density of the sp^3 quantum defects. At a low doping level, the kinetics of E_{11} excitons are determined by a diffusion-limited first-order decay process and exciton−exciton interactions, similar to those in pristine nanotubes. The introduction of more sp^3 quantum defects eventually makes the trapping of E_{11} excitons at the quantum defect sites the predominant decay channel, which leads to the accumulation of excitons in the quantum defect states and depletion of the ground state. These findings provide critical knowledge not only for the design of quantum defects that would enable stable and bright emission for quantum information[2,7,26] and bioimaging[27] applications but also for the development of SWCNT-based ultracompact nanolasers operating at the telecom bands.[28]

METHODS

Sample Preparation. CoMoCAT SG65i SWCNTs (Southwest Nanotechnologies, lot no. SG65i-L39) were dispersed in 1% w/v sodium deoxycholate (DOC, Sigma-Aldrich, >97%) aqueous solution using tip sonication at 8 W (Qsonica S-4000) for an hour. Chirality-enriched (6,5) SWCNTs were then isolated by an aqueous two-phase extraction method.[1] The sorted SWCNT solution was filtrated in a centrifugal filter (Amicon Ultra-15, 100 kDa cutoff) to exchange the SWCNTs into 1 wt %/v DOC in D_2O (Cambridge Isotope Laboratories, Inc., 99.8%). The purity and concentration of the (6,5) SWCNT solutions were determined by UV−vis-NIR absorption spectroscopy (Lambda 1050, PerkinElmer).

For the subsequent functionalization, the chirality sorted (6,5)-SWCNT solutions were diluted to an optical density of 0.3 at 988 nm

DOI: 10.1021/acsnano.9b06279
ACS Nano 2019, 13, 13264−13270

using 1 wt %/v sodium dodecyl sulfate (SDS, Sigma-Aldrich, > 98.5%) in D_2O. The sp^3 quantum defects were incorporated into the (6,5) SWCNT sidewalls by reacting the SWCNTs with 4-nitrobenzenediazonium tetrafluoroborate. Specifically, the mixtures were illuminated for 20 min using the 565 nm light from a Nanolog spectrometer (Horiba Jobin Yvon). After overnight incubation of the doped SWCNT solutions, they were filtrated using 1 wt %/v DOC–D_2O to concentrate the solution by 4 times for the TA measurements. Samples for the TA measurements were placed in 2 mm thick cuvettes.

ASSOCIATED CONTENT

Supporting Information

The Supporting Information is available free of charge on the ACS Publications website at DOI: 10.1021/acsnano.9b06279.

Optical and AFM characterizations of SWCNTs; calculation of defect densities; description of the kinetic model and fitting method; representative TA spectra and fitting results of the doped SWCNTs; calculation of the average distance between two sp^3 quantum defects in SWCNTs; pump intensity dependence of the TA signals; comparison of rates between exciton–exciton annihilation and trapping at quantum defects (PDF)

AUTHOR INFORMATION

Corresponding Author

*E-mail: xuedan.ma@anl.gov.

ORCID

YuHuang Wang: 0000-0002-5664-1849

David J. Gosztola: 0000-0003-2674-1379

Xuedan Ma: 0000-0002-3163-1249

Notes

The authors declare no competing financial interest.

ACKNOWLEDGMENTS

Use of the Center for Nanoscale Materials, an Office of Science user facility, was supported by the U.S. Department of Energy, Office of Science, Office of Basic Energy Sciences, under Contract No. DE-AC02-06CH11357. X.M. acknowledges support from the National Science Foundation DMR Program under Award No. DMR-1905990. Y.H.W. gratefully acknowledges support from NSF PHY-1839165. M.K. acknowledges the Millard and Lee Alexander Fellowship in Chemistry from the University of Maryland. We thank Libai Huang for helpful discussion regarding the TA measurements.

REFERENCES

(1) Piao, Y.; Meany, B.; Powell, L. R.; Valley, N.; Kwon, H.; Schatz, G. C.; Wang, Y. Brightening of Carbon Nanotube Photoluminescence through the Incorporation of sp^3 Defects. *Nat. Chem.* **2013**, *5*, 840–845.

(2) He, X.; Hartmann, N. F.; Ma, X.; Kim, Y.; Ihly, R.; Blackburn, J. L.; Gao, W.; Kono, J.; Yomogida, Y.; Hirano, A.; Tanaka, T.; Kataura, H.; Htoon, H.; Doorn, S. K. Tunable Room-Temperature Single-Photon Emission at Telecom Wavelengths from sp^3 Defects in Carbon Nanotubes. *Nat. Photonics* **2017**, *11*, 577–582.

(3) Kwon, H.; Furmanchuk, A.; Kim, M.; Meany, B.; Guo, Y.; Schatz, G. C.; Wang, Y. Molecularly Tunable Fluorescent Quantum Defects. *J. Am. Chem. Soc.* **2016**, *138*, 6878–6885.

(4) Miyauchi, Y.; Iwamura, M.; Mouri, S.; Kawazoe, T.; Ohtsu, M.; Matsuda, K. Brightening of Excitons in Carbon Nanotubes on Dimensionality Modification. *Nat. Photonics* **2013**, *7*, 715–719.

(5) Ma, X.; Adamska, L.; Yamaguchi, H.; Yalcin, S. E.; Tretiak, S.; Doorn, S. K.; Htoon, H. Electronic Structure and Chemical Nature of Oxygen Dopant States in Carbon Nanotubes. *ACS Nano* **2014**, *8*, 10782–10789.

(6) Ghosh, S.; Bachilo, S. M.; Simonette, R. A.; Beckingham, K. M.; Weisman, R. B. Oxygen Doping Modifies Near-Infrared Band Gaps in Fluorescent Single-Walled Carbon Nanotubes. *Science* **2010**, *330*, 1656–1659.

(7) Ma, X.; Hartmann, N. F.; Baldwin, J. K. S.; Doorn, S. K.; Htoon, H. Room-Temperature Single-Photon Generation from Solitary Dopants of Carbon Nantoubes. *Nat. Nanotechnol.* **2015**, *10*, 671–675.

(8) Iwamura, M.; Akizuki, N.; Miyauchi, Y.; Mouri, S.; Shaver, J.; Gao, Z.; Cognet, L.; Lounis, B.; Matsuda, K. Nonlinear Photoluminescence Spectroscopy of Carbon Nanotubes with Localized Exciton States. *ACS Nano* **2014**, *8*, 11254–11260.

(9) Hartmann, N. F.; Velizhanin, K. A.; Haroz, E. H.; Kim, M.; Ma, X.; Wang, Y.; Htoon, H.; Doorn, S. K. Photoluminescence Dynamics of Aryl sp^3 Defect States in Single-Walled Carbon Nanotubes. *ACS Nano* **2016**, *10*, 8355–8365.

(10) Kim, Y. L.; Jung, H. Y.; Park, S.; Li, B.; Liu, F.; Hao, J.; Kwon, Y.-K.; Jung, Y. J.; Kar, S. Voltage-Switchable Photocurrents in Single-Walled Carbon Nanotube–Silicon Junctions for Analog and Digital Optoelectronics. *Nat. Photonics* **2014**, *8*, 239–243.

(11) Khasminskaya, S.; Pyatkov, F.; Słowik, K.; Ferrari, S.; Kahl, O.; Kovalyuk, V.; Rath, P.; Vetter, A.; Hennrich, F.; Kappes, M. M.; Gol'tsman, G.; Korneev, A.; Rockstuhl, C.; Krupke, R.; Pernice, W. H. P. Fully Integrated Quantum Photonic Circuit with an Electrically Driven Light Source. *Nat. Photonics* **2016**, *10*, 727–733.

(12) Graf, A.; Held, M.; Zakharko, Y.; Tropf, L.; Gather, M. C.; Zaumseil, J. Electrical Pumping and Tuning of Exciton-Polaritons in Carbon Nanotube Microcavities. *Nat. Mater.* **2017**, *16*, 911–917.

(13) Zhu, Z.; Crochet, J.; Arnold, M. S.; Hersam, M. C.; Ulbricht, H.; Resasco, D.; Hertel, T. Pump-Probe Spectroscopy of Exciton Dynamics in (6,5) Carbon Nanotubes. *J. Phys. Chem. C* **2007**, *111*, 3831–3835.

(14) Styers-Barnett, D. J.; Ellison, S. P.; Mehl, B. P.; Westlake, B. C.; House, R. L.; Park, C.; Wise, K. E.; Papanikolas, J. M. Exciton Dynamics and Biexciton Formation in Single-Walled Carbon Nanotubes Studied with Femtosecond Transient Absorption Spectroscopy. *J. Phys. Chem. C* **2008**, *112*, 4507–4516.

(15) Yuma, B.; Berciaud, S.; Besbas, J.; Shaver, J.; Santos, S.; Ghosh, S.; Weisman, R. B.; Cognet, L.; Gallart, M.; Ziegler, M.; Honerlage, M.; Lounis, B.; Gilliot, P. Biexciton, Single Carrier, and Trion Generation Dynamics in Single-Walled Carbon Nanotubes. *Phys. Rev. B: Condens. Matter Mater. Phys.* **2013**, *87*, 205412.

(16) Santos, S. M.; Yuma, B.; Berciaud, S.; Shaver, J.; Gallart, M.; Gilliot, P.; Cognet, L.; Lounis, B. All-Optical Trion Generation in Single-Walled Carbon Nanotubes. *Phys. Rev. Lett.* **2011**, *107*, 187401.

(17) Eckstein, K. H.; Hartleb, H.; Achsnich, M. M.; Schöppler, F.; Hertel, T. Localized Charges Control Exciton Energetics and Energy Dissipation in Doped Carbon Nanotubes. *ACS Nano* **2017**, *11*, 10401–10408.

(18) Park, J.; Deria, P.; Olivier, J.-H.; Therien, M. J. Fluence-Dependent Singlet Exciton Dynamics in Length-Sorted Chirality-Enriched Single-Walled Carbon Nanotubes. *Nano Lett.* **2014**, *14*, 504–411.

(19) Korovyanko, O. J.; Sheng, C.-X.; Vardeny, Z. V.; Dalton, A. B.; Baughman, R. H. Ultrafast Spectroscopy of Excitons in Single-Walled Carbon Nanotubes. *Phys. Rev. Lett.* **2004**, *92*, 017403.

(20) Berera, R.; van Grondelle, R.; Kennis, J. T. M. Ultrafast Transient Absorption Spectroscopy: Principles and Application to Photosynthetic Systems. *Photosynth. Res.* **2009**, *101*, 105–118.

(21) Noginov, M. A.; Zhu, G.; Bahoura, M.; Small, C. E.; Davison, C.; Adegoke, J.; Drachev, V. P.; Nyga, P.; Shalaev, V. M. Enhancement of Spontaneous and Stimulated Emission of a Rhodamine 6G Dye by an Ag Aggregate. *Phys. Rev. B: Condens. Matter Mater. Phys.* **2006**, *74*, 184203.

(22) Yan, M.; Rothberg, L. J.; Papadimitrakopoulos, F.; Galvin, M. E.; Miller, T. M. Spatially Indirect Excitons as Primary Photoexcitations in Conjugated Polymers. *Phys. Rev. Lett.* **1994**, *72*, 1104–1107.

DOI: 10.1021/acsnano.9b06279
ACS Nano 2019, 13, 13264–13270

(23) Klimov, V. I.; Mikhailovsky, A. A.; Xu, S.; Malko, A.; Hollingsworth, J. A.; Leatherdale, C. A.; Eisler, H.-J.; Bawendi, M. G. Optical Gain and Stimulated Emission in Nanocrystal Quantum Dots. *Science* **2000**, *290*, 314−317.
(24) Harrah, D. M.; Schneck, J. R.; Green, A. A.; Hersam, M. A.; Ziegler, L. D.; Swan, A. K. Intensity-Dependent Exciton Dynamics of (6,5) Single-Walled Carbon Nanotubes: Momentum Selection Rules, Diffusion, and Nonlinear Interactions. *ACS Nano* **2011**, *5*, 9898−9906.
(25) Lüer, L.; Hoseinkhani, S.; Polli, D.; Crochet, J.; Hertel, T.; Lanzani, G. Size and Mobility of Excitons in (6, 5) Carbon Nanotubes. *Nat. Phys.* **2009**, *5*, 54−58.
(26) Saha, A.; Gifford, B. J.; He, X.; Ao, G.; Zheng, M.; Kataura, H.; Htoon, H.; Kilina, S.; Tretiak, S.; Doorn, S. K. Narrow-Band Single-Photon Emission through Selective Aryl Functionalization of Zigzag Carbon Nanotubes. *Nat. Chem.* **2018**, *10*, 1089−1095.
(27) Hong, G.; Diao, S.; Antaris, A. L.; Dai, H. Carbon Nanomaterials for Biological Imaging and Nanomedicinal Therapy. *Chem. Rev.* **2015**, *115*, 10816−10906.
(28) Gaufrès, E.; Izard, N.; Le Roux, X.; Marris-Morini, D.; Kazaoui, S.; Cassan, E.; Vivien, L. Optical Gain in Carbon Nanotubes. *Appl. Phys. Lett.* **2010**, *96*, 231105.

DOI: 10.1021/acsnano.9b06279
ACS Nano 2019, 13, 13264−13270